

# The Continuous Synthesis of 2-(2'-Hydroxy-5'-Methylphenyl)Benzotriazole over Cu/ $\gamma$ -Al<sub>2</sub>O<sub>3</sub>

L. Yan<sup>a</sup>, L. Si<sup>b</sup>, Q. Tao<sup>a</sup>, L. Liu<sup>a</sup>, B. Wang<sup>a, c, d, \*, \*\*</sup>, and Y. Li<sup>a, c, d, \*\*</sup>

<sup>a</sup>School of Chemical Engineering and Technology, Tianjin University, Tianjin, 300350 P.R. China

<sup>b</sup>Disha Pharmaceutical Group Co. Ltd., Tianjin, P.R. China

<sup>c</sup>Collaborative Innovation Center of Chemical Science and Engineering (Tianjin), Tianjin, 300072 P.R. China

<sup>d</sup>Tianjin Engineering Research Center of Functional Fine Chemicals, Tianjin, P.R. China

\*e-mail: bwwang@tju.edu.cn

\*\*e-mail: liyang777@tju.edu.cn

Received January 27, 2019; revised April 8, 2019; accepted May 13, 2019

**Abstract**—The samples of 20% Cu/ $\gamma$ -Al<sub>2</sub>O<sub>3</sub>, 20% Co/ $\gamma$ -Al<sub>2</sub>O<sub>3</sub> and 20% Ni/ $\gamma$ -Al<sub>2</sub>O<sub>3</sub> were prepared as hydrogenation catalysts for continuous synthesis of 2-(2'-hydroxy-5'-methylphenyl)benzotriazole. The best yield (86.62%) was afforded by the 20% Cu/ $\gamma$ -Al<sub>2</sub>O<sub>3</sub> catalyst. The characterizations results obtained for the 20% Cu/ $\gamma$ -Al<sub>2</sub>O<sub>3</sub> sample confirmed that Cu particles are evenly distributed over the surface of  $\gamma$ -Al<sub>2</sub>O<sub>3</sub>. A reduction of acid sites in the catalyst favored the selectivity to 2-(2'-hydroxy-5'-methylphenyl)benzotriazole. Furthermore, the effect of Cu content, reaction temperature, hydrogen pressure and liquid hourly space velocity was studied. Finally, 2-(2'-hydroxy-5'-methylphenyl)benzotriazole in 86.62% yield was attained under the optimized conditions.

**Keywords:** catalytic hydrogenation, benzotriazole, transition metal catalysts

**DOI:** 10.1134/S0023158419050124

## INTRODUCTION

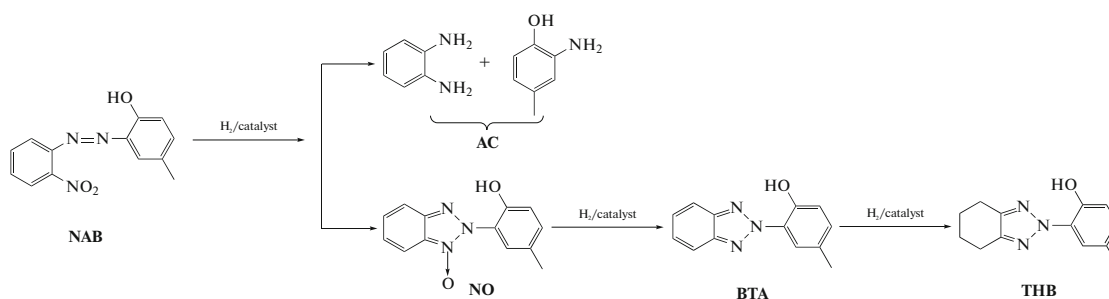
Benzotriazole ultraviolet absorbers, as a class of the light stabilizers, are used to prevent degradation of polymer materials [1, 2]. Accordingly, the synthesis of benzotriazoles has also attracted worldwide attention [3–6]. Generally, a two-step preparation of benzotriazoles conventionally involves synthesis and reductive cyclization of azo dyes intermediate. Synthesis of azo dyes is quite mature, including microwave irradiation, solid phase and solution reaction methods [7–9]. However, the reductive cyclization of azo dyes, as the key step in the preparation of benzotriazoles, is difficult to control because it is accompanied by side reactions [10–14]. At present, the reductive cyclization is mainly conducted by using zinc powder, hydrazine hydrate, SmI<sub>2</sub>, or sulfides [15–18]. However, using these reagents has certain disadvantages. For instance, while zinc powder reduction method is widely applied in the industry with a satisfactory yield of benzotriazoles, it is associated with serious environmental problems [16, 18, 19]. Considering the cost and environmental consequences, the catalytic hydrogenation appears as an ideal alternative because it can be expected that the catalytic hydrogenation generates water as the only by-product [20].

From earlier patents describing catalytic hydrogenation the information on attractive yields of benzotriazoles can be derived [21–23]. However, no detailed explanation of the experimental results could be found in patent reports. Besides, in these experiments the catalytic hydrogenation was carried out in a flask or autoclave and the results could be hardly scaled to the industrial production of benzotriazoles. Thus, there is a need for an efficient and economically feasible method of synthesis of benzotriazoles. In a number of studies, hydrogenation of 2-nitro-2'-hydroxy-5'-methylazobenzene (NAB) was described [24–26]. In our previous works [27], the continuous catalytic hydrogenation of NAB to 2-(2'-hydroxy-5'-methylphenyl)benzotriazole (BTA) was investigated by using Pd/ $\gamma$ -Al<sub>2</sub>O<sub>3</sub> as a catalyst. It was found that Pd-based catalyst exhibited an excellent performance. But the additional base was required in this reaction to restrain the generation of amino by-products [10, 28]. To overcome this obstacle, solid base-hydrogenation bifunctional catalysts were employed and the effect of different alkali metals over Pd/ $\gamma$ -Al<sub>2</sub>O<sub>3</sub> was studied [29, 30]. Although the satisfactory results were obtained, it was desirable to find a catalytic system as an alternative to noble metal catalyst used in this reaction and optimize the reaction conditions. Less expensive transition

metal systems were developed as catalysts for the continuous catalytic hydrogenation, but results obtained were far from ideal [27]. Therefore, the exploration of high-performance transition metal catalysts remains an important challenge.

In the present work, we focused on the preparation of a series of transition metal systems including Cu/ $\gamma$ -Al<sub>2</sub>O<sub>3</sub>, Co/ $\gamma$ -Al<sub>2</sub>O<sub>3</sub> and Ni/ $\gamma$ -Al<sub>2</sub>O<sub>3</sub> as catalysts for the continuous catalytic hydrogenation of NAB to BTA (Scheme 1) [30]. Among these, Cu/ $\gamma$ -Al<sub>2</sub>O<sub>3</sub> showed

excellent catalytic performance with 86.62% yield of BTA. The catalysts were characterized by X-ray diffraction (XRD), transmission electron microscopy (TEM), Brunauer–Emmer–Teller (BET) surface area measurements and temperature programmed desorption of ammonia (NH<sub>3</sub>-TPD) to discuss the structure-activity relationship. Moreover, reaction parameters were optimized in terms of Cu content, reaction temperature, hydrogen pressure and liquid hourly space velocity (LHSV).



Scheme 1. Catalytic hydrogenation of NAB.

## EXPERIMENTAL

### Materials

Nitrate hydrates Cu(NO<sub>3</sub>)<sub>2</sub> · 3H<sub>2</sub>O (analytical reagent (AR)), Co(NO<sub>3</sub>)<sub>2</sub> · 6H<sub>2</sub>O (AR) and Ni(NO<sub>3</sub>)<sub>2</sub> · 6H<sub>2</sub>O (AR) were provided by Tianjin Ruijinte Chemical Co., Ltd. (China). Toluene (AR), triethylamine (AR) and anhydrous sodium carbonate (AR) were purchased from Tianjin Jiangtian Chemical Co., Ltd. (China). Pseudo-boehmite was obtained from Jiangyan Chemical Auxiliary Factory (China). 2-Nitroaniline (AR) and *p*-Cresol (AR) were respectively gained from Tianjin Yuanli Chemical Co., Ltd. and Tianjin Guangfu Technology Development Co., Ltd. (China). Commercially available reagents were used without further purification. 2-Nitro-2'-hydroxy-5'-methylazobenzene (≥ 90%, as determined by high performance liquid chromatography (HPLC) was produced by diazotization and coupling reaction.

### Catalyst Preparation

The transition metal catalysts were prepared by the co-precipitation-kneading method [27, 31–33]. To prepare the 20% Cu/ $\gamma$ -Al<sub>2</sub>O<sub>3</sub> (20 wt. % Cu in the catalyst) 48.32 g of Cu(NO<sub>3</sub>)<sub>2</sub> · 3H<sub>2</sub>O and 23.32 g of Na<sub>2</sub>CO<sub>3</sub> were separately dissolved into 500 mL deionized water to form the solutions A and solution B. Both of the solution A and B were simultaneously dropped slowly into a big beaker with 500 mL deionized water under mechanical stirring at room temperature. The pH value of the reaction mixture was maintained

between 7–8 as monitored during the dropping process. Then, the solution was stirred for 1 h and aged for another 1 h. The mixture was filtered, washed and dried at 120°C for 6 h. Adding 76.8 g of pseudo-boehmite and a moderate amount of water pulverized the solid. Then, the mixture was kneaded adequately and then extruded by an extrusion machine. After drying at 120°C for 6 h, the bars were calcined at 550°C for 4 h in a muffle and then the obtained precursor was activated at 240°C at a hydrogen pressure of 1.0 MPa for 4 h. Other catalysts were prepared by a similar process applying the activation temperatures of 400 and 360°C for Co/ $\gamma$ -Al<sub>2</sub>O<sub>3</sub> and Ni/ $\gamma$ -Al<sub>2</sub>O<sub>3</sub>, respectively.

### Catalyst Characterization

The XRD patterns were measured with a Rigaku D/max 2500 (Rigaku Corporation, Japan) using CuK $\alpha$  X-ray radiation (40 kV, 100 mA). TEM micrographs were performed on a Tecnai G2 F20 high-resolution analytical electron microscope (FEI, Netherlands) operating at an electron beam voltage of 200 kV. The specific surface areas were determined by BET method with N<sub>2</sub> adsorption-desorption measurements at 77.4 K using a NOVA 2000e analyzer (Quantachrome Instruments, USA). NH<sub>3</sub>-TPD was carried out on a TP-5000 instrument (XQ, China) equipped with a thermal conductivity detector. The samples were treated under argon at 800°C for 2 h, cooled down to 25°C in flowing argon, and then treated with flowing NH<sub>3</sub> for 10 min at 30°C. Finally, the sample

**Table 1.** The catalytic hydrogenation of NAB over transition metal catalysts

| Catalysts  | Conversion of NAB, % | Selectivity, % |       |       |      |        |
|--|----------------------|----------------|-------|-------|------|--------|
|  |                      | AC             | NO    | BTA   | THB  | others |
| 20% Cu/ $\gamma$ -Al <sub>2</sub> O <sub>3</sub> | 99.52                | 0.45           | 1.44  | 87.04 | 1.31 | 9.76   |
| 20% Co/ $\gamma$ -Al <sub>2</sub> O <sub>3</sub> | 98.85                | 58.34          | 25.70 | 2.47  | 0.76 | 12.73  |
| 20% Ni/ $\gamma$ -Al <sub>2</sub> O <sub>3</sub> | 100.00               | 10.20          | 5.84  | 71.83 | —    | 12.13  |

Reaction conditions: solvent—toluene, base—triethylamine (molar ratio of NAB : triethylamine = 1 : 2), catalyst—40 mL, reaction temperature—120°C, hydrogen pressure—2.5 MPa, and LHSV—0.23 h<sup>-1</sup>.

was heated to 700°C with a ramping temperature of 15°C/min.

catalysts were characterized by XRD, TEM, BET and NH<sub>3</sub>-TPD techniques.

### Catalytic Reactions

The catalytic hydrogenation of NAB was accomplished under the requisite temperature, hydrogen pressure and LHSV in a fixed bed reactor with an inner diameter of 15 mm and a length of 650 mm. The reaction was carried out using 40 mL catalyst with a particle size of 3 mm. A 5 wt. % solution of NAB in toluene was fed into the reactor by a tranquil flow pump. A proportion integration differentiation cascade controller regulated the temperature inside the catalyst layer. Gas valves controlled the hydrogen pressure. The analysis of sample was collected continuously and the sampling frequency was set to one acquisition per hour. The components of reaction mixture were analyzed using HPLC with a column of Extend C<sub>18</sub> (250 × 4.6 mm, 10 μm, Agilent technologies, USA).

## RESULTS AND DISCUSSION

### Catalyst Selection

Initially, 20% Cu/ $\gamma$ -Al<sub>2</sub>O<sub>3</sub>, 20% Co/ $\gamma$ -Al<sub>2</sub>O<sub>3</sub> and 20% Ni/ $\gamma$ -Al<sub>2</sub>O<sub>3</sub> were employed for the catalytic hydrogenation of NAB. The results are presented in Table 1. These catalysts displayed excellent activities in the catalytic hydrogenation with conversions of NAB exceeding 98%. However, three catalysts showed considerable variations in the BTA selectivity. Selectivity for BTA over 20% Cu/ $\gamma$ -Al<sub>2</sub>O<sub>3</sub> was as high as 87.04%. When 20% Ni/ $\gamma$ -Al<sub>2</sub>O<sub>3</sub> was applied for the hydrogenation, the selectivity for BTA was 71.83%. In the presence of 20% Co/ $\gamma$ -Al<sub>2</sub>O<sub>3</sub> the main products were 2-amino-*p*-cresol, *o*-phenylenediamine (AC, amino compounds) and 2-(2'-hydroxy-5'-methylphenyl)benzotriazole N-oxide (NO). The level of selectivity for AC (58.34%) indicates that the azo bond was broken [10]. From the above results it can be inferred that the 20% Cu/ $\gamma$ -Al<sub>2</sub>O<sub>3</sub> catalyst showed the best catalytic performance. To further explore the structure-activity relationship of 20% Cu/ $\gamma$ -Al<sub>2</sub>O<sub>3</sub>, 20% Co/ $\gamma$ -Al<sub>2</sub>O<sub>3</sub> and 20% Ni/ $\gamma$ -Al<sub>2</sub>O<sub>3</sub>, the

### Catalyst Characterization

**The XRD analysis.** The XRD patterns of 20% Cu/ $\gamma$ -Al<sub>2</sub>O<sub>3</sub>, 20% Co/ $\gamma$ -Al<sub>2</sub>O<sub>3</sub> and 20% Ni/ $\gamma$ -Al<sub>2</sub>O<sub>3</sub> catalysts are shown in Fig. 1. The three peaks at 37°, 46° and 67° corresponding to (111), (400) and (440) planes of  $\gamma$ -Al<sub>2</sub>O<sub>3</sub> respectively that are present in each sample are consistent with the formation of the  $\gamma$ -Al<sub>2</sub>O<sub>3</sub> phase [27, 29, 34]. Furthermore, for 20% Cu/ $\gamma$ -Al<sub>2</sub>O<sub>3</sub>, the sharp diffraction maxima at 43°, 50° and 74° were observed assignable to the diffraction peaks of metal Cu (111), (200) and (220) planes, respectively (Fig. 1a) [35, 36]. The signal at 90° can also be attributed to metal Cu (111) crystal face (JCPDS 04-0836). XRD pattern of the 20% Co/ $\gamma$ -Al<sub>2</sub>O<sub>3</sub> catalyst showed characteristic peaks at 48°, 76° and 93° corresponding respectively to (101), (110) and (112) planes of metal Co crystallites (JCPDS 29-0021 and JCPDS 05-0727) (Fig. 1b). Meanwhile, the diffraction peak at 45° is assigned to the (110) crystal face of Al-Co phase (JCPDS 29-0021). A diffraction peak attributable to Al<sub>2</sub>O structure is also found at 52° (JCPDS 75-0277). XRD profile of the 20% Ni/ $\gamma$ -Al<sub>2</sub>O<sub>3</sub> catalyst clearly showed four peaks at 45°, 52°, 76° and 93° belong to (111), (200), (220) and (311) planes of Ni<sup>0</sup> respectively (JCPDS 04-0850 and JCPDS 03-1051) (Fig. 1c). Therefore it emerges that metal Cu, Co and Ni were successfully supported on the surface of  $\gamma$ -Al<sub>2</sub>O<sub>3</sub> and the presence of zero-charged metals can be recognized in all samples suggesting the existence of active sites for the catalytic hydrogenation.

**TEM analysis.** Fig. 2 presents the images illustrating the morphological features of 20% Cu/ $\gamma$ -Al<sub>2</sub>O<sub>3</sub>, 20% Co/ $\gamma$ -Al<sub>2</sub>O<sub>3</sub> and 20% Ni/ $\gamma$ -Al<sub>2</sub>O<sub>3</sub> catalysts. The average diameter of Cu particles was found to be 3.29 nm (Fig. 2a). However, the size of Co particles is about 79.66 nm and it appears that the initial crystals are formed into polycrystalline aggregates shown in Fig. 2b. Partial agglomeration of Ni particles

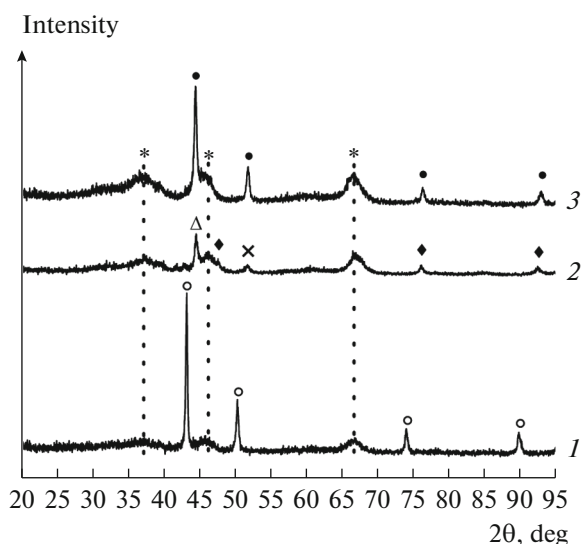


**Fig. 1.** The XRD patterns: (1) 20% Cu/ $\gamma$ -Al<sub>2</sub>O<sub>3</sub>, (2) 20% Co/ $\gamma$ -Al<sub>2</sub>O<sub>3</sub>, and (3) 20% Ni/ $\gamma$ -Al<sub>2</sub>O<sub>3</sub>. Symbols: \*  $\gamma$ -Al<sub>2</sub>O<sub>3</sub>, ○ Cu, △ Al-Co phase, ◆ Co, × Al<sub>2</sub>O<sub>3</sub>, ● Ni.

can account for an average diameter of 21.02 nm calculated for polycrystalline spheroids in the 20% Ni/ $\gamma$ -Al<sub>2</sub>O<sub>3</sub> catalyst (Fig. 2c). The phenomenon of particle aggregation may be related to a high reduction temperature [37]. The differences in the dispersion degree may also significantly affect the catalytic performance [38, 39]. The presence of metal nanoparticles loaded on the surface of  $\gamma$ -Al<sub>2</sub>O<sub>3</sub> agrees with the XRD results.

**BET analysis.** The BET surface area, total pore volume and average pore diameter were characterized by N<sub>2</sub> adsorption–desorption measurements. Table 2 shows that the BET surface area and total pore volume of  $\gamma$ -Al<sub>2</sub>O<sub>3</sub> are 252 m<sup>2</sup>/g and 0.70 cm<sup>3</sup>/g, respectively. The BET surface area and the pore volume calculated for Cu, Co and Ni catalysts supported on  $\gamma$ -Al<sub>2</sub>O<sub>3</sub> show a small reduction caused by occlusion of metals in pore voids. The structural properties of the three

catalysts seem to be similar. The lowest BET surface area (186 m<sup>2</sup>/g) was found for the 20% Cu/ $\gamma$ -Al<sub>2</sub>O<sub>3</sub> sample, whereas the highest value (212 m<sup>2</sup>/g) was recorded for the 20% Co/ $\gamma$ -Al<sub>2</sub>O<sub>3</sub> catalyst. The information outline above indicates that the structural properties are not the main factors that govern the catalytic performance.

**NH<sub>3</sub>-TPD analysis.** NH<sub>3</sub>-TPD was carried out to study the acidity of the three catalysts. As can be readily recognized in Fig. 3, all catalysts exhibit two ammonia desorption peaks. It appears that the amount of acid sites in the 20% Cu/ $\gamma$ -Al<sub>2</sub>O<sub>3</sub> sample is lower than that in other two catalysts. According to the reports [10], the reductive cyclization of NAB proceeded readily in alkaline environment. The acid sites of the catalyst may cause the cleavage of the N=N bond, which is not favorable for the progress of the reaction. The results are consistent with the fact that a high selectivity for BTA was observed in the presence of 20% Cu/ $\gamma$ -Al<sub>2</sub>O<sub>3</sub> (Table 1).

According to the results derived from XRD, TEM, BET and NH<sub>3</sub>-TPD measurements, Cu particles were uniformly dispersed in the 20% Cu/ $\gamma$ -Al<sub>2</sub>O<sub>3</sub> catalyst and the amount of acid sites was less than in other two catalysts. A high fraction of copper exposed and a moderate acidity can be the main factors responsible for a good performance of the 20% Cu/ $\gamma$ -Al<sub>2</sub>O<sub>3</sub> catalyst. It can also be deduced from the foregoing that BET surface area of catalysts has little effect on the catalytic hydrogenation.

#### Catalytic Hydrogenation of NAB to BTA

In order to further improve the conversion of NAB and selectivity for BTA a series of reaction parameters including Cu content, reaction temperature, hydrogen pressure and LHSV were optimized with the results shown in Fig. 4.

At the first step, the effect of copper loading on the continuous catalytic hydrogenation of NAB was explored. Based on the data shown in Fig. 4a, increas-

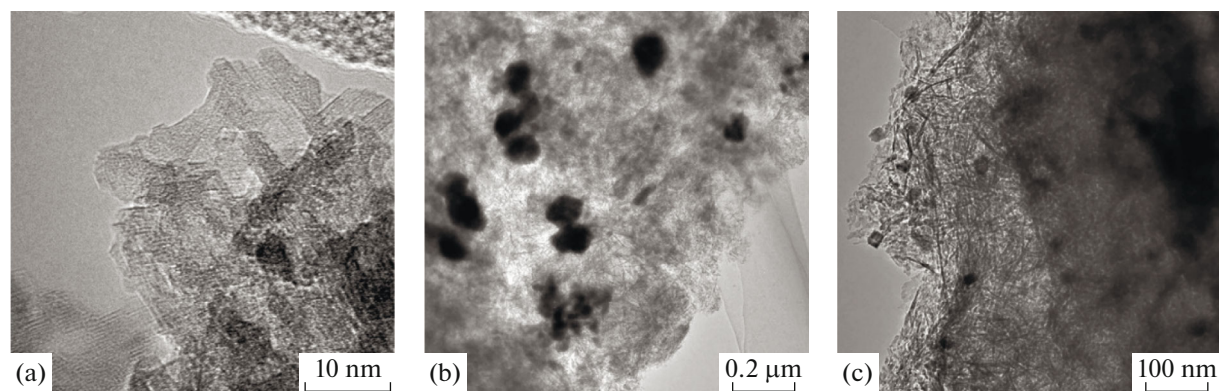


**Fig. 2.** TEM images of (a) 20% Cu/ $\gamma$ -Al<sub>2</sub>O<sub>3</sub>, (b) 20% Co/ $\gamma$ -Al<sub>2</sub>O<sub>3</sub>, and (c) 20% Ni/ $\gamma$ -Al<sub>2</sub>O<sub>3</sub>.

**Table 2.** The structure properties of support and different catalysts

| Catalysts  | $S_{\text{BET}}$ , m <sup>2</sup> /g* | $V_{\text{total}}$ , cm <sup>3</sup> /g** | $D_{\text{average}}$ , nm*** |
|--|---------------------------------------|---|------------------------------|
| 20% Cu/ $\gamma$ -Al <sub>2</sub> O <sub>3</sub> | 186                                   | 0.46                                      | 4.94                         |
| 20% Co/ $\gamma$ -Al <sub>2</sub> O <sub>3</sub> | 212                                   | 0.56                                      | 5.32                         |
| 20% Ni/ $\gamma$ -Al <sub>2</sub> O <sub>3</sub> | 202                                   | 0.60                                      | 5.91                         |
| $\gamma$ -Al <sub>2</sub> O <sub>3</sub>         | 252                                   | 0.70                                      | 5.59                         |

\* BET surface area.

\*\* Total pore volume.

\*\*\* Average pore diameter.

ing the Cu content from 10 to 20% leads to an improvement both in conversion of NAB and selectivity for BTA was observed. This effect is probably due to an increase in the population of active sites. However when the Cu content was further increased to 25% the conversion for NAB decreased to a value of 87.73% with a concomitant reduction of the BTA selectivity. It can be speculated that the deterioration of the catalytic performance can be accounted for by the particle agglomeration that is caused by the presence of excessive amounts of Cu [40]. Obviously, 20% Cu/ $\gamma$ -Al<sub>2</sub>O<sub>3</sub> is the optimal catalyst, which afforded 86.62% yield of BTA.

At the next step, the effect of the reaction temperature was studied (Fig. 4b). As the reaction was raised from 80 to 120°C, the conversion of NAB increased from 56.21 to 99.52% whereas the selectivity for BTA increased from 18.09 to 87.04%. Between the reaction temperatures of 120 and 130°C, the conversion of NAB remained at a level near 99%, however, the selectivity for BTA declined to 74.11%. A possible explanation is that the selectivity for by-products also increases with increasing temperature. Thus, a reaction temperature of 120°C was found to be optimal and was further used in the present work.

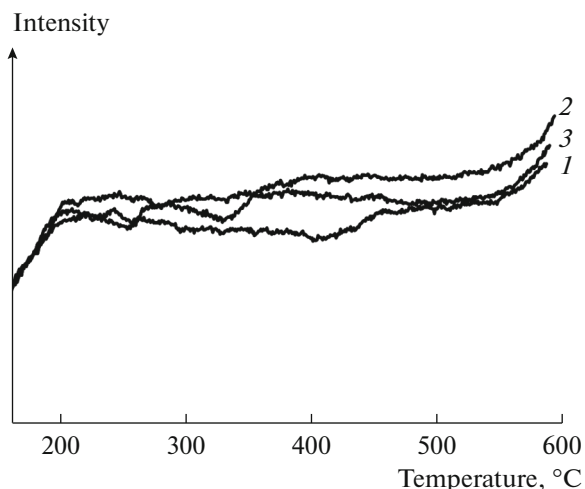


**Fig. 3.** NH<sub>3</sub>-TPD profiles: (1) 20% Cu/ $\gamma$ -Al<sub>2</sub>O<sub>3</sub>, (2) 20% Co/ $\gamma$ -Al<sub>2</sub>O<sub>3</sub> and (3) 20% Ni/ $\gamma$ -Al<sub>2</sub>O<sub>3</sub>.

The influence of hydrogen pressure on the hydrogenation reduction of NAB was also explored (Fig. 4c). As reaction pressure was raised from 2.0 to 3.0 MPa, the conversion of NAB increased from 95.14 to 99.52% and then remained nearly constant. Meanwhile, the selectivity of BTA was found to parallel the conversion trend reaching a value of 87.63%. Considering the production cost, 2.5 MPa hydrogen pressure was chosen as the optimal reaction pressure with 86.62% BTA yield.

Finally, the influence of LHSV was also investigated (Fig. 4d). Normally, the LHSV directly affects the residence time of raw material on the catalyst bed. The smaller LHSV lead to longer residence times, which may result in the increase of by-products selectivity. However, excessively large LHSV can cause a decline in the conversion of NAB. As shown in Fig. 4d, when the LHSV was increased from 0.15 to 0.30 h<sup>-1</sup>, the conversion of NAB gradually decreased to 90.01% whereas the selectivity of BTA first increased from 73.56 to 87.04% and then decreased to 84.23%. As a result, a value of LHSV 0.23 h<sup>-1</sup> that afforded 86.62% BTA yield was considered as the best choice.

On the basis of the foregoing discussion the optimal reaction conditions were chosen: catalyst – 20% Cu/ $\gamma$ -Al<sub>2</sub>O<sub>3</sub>, solvent—toluene, base—triethylamine (molar ratio of NAB : triethylamine = 1 : 2). The reactor operates at a temperature of 120°C, a hydrogen pressure of 2.5 MPa, and a LHSV of 0.23 h<sup>-1</sup>. Under the above conditions, the continuous catalytic hydrogenation of NAB proceeded effectively to yield 87.04% of BTA at 99.52% NAB conversion.

## CONCLUSIONS

The samples of 20% Cu/ $\gamma$ -Al<sub>2</sub>O<sub>3</sub>, 20% Co/ $\gamma$ -Al<sub>2</sub>O<sub>3</sub> and 20% Ni/ $\gamma$ -Al<sub>2</sub>O<sub>3</sub> were prepared as hydrogenation catalysts for continuous synthesis of 2-(2'-hydroxy-5'-methylphenyl)benzotriazole in a fixed bed reactor. These catalysts were characterized by XRD, TEM, BET and NH<sub>3</sub>-TPD to explain the structure-activity relationship. As evidenced by TEM images of the 20% Cu/ $\gamma$ -Al<sub>2</sub>O<sub>3</sub> sample Cu particles are evenly distributed over the surface of  $\gamma$ -Al<sub>2</sub>O<sub>3</sub>. The other two catalysts show signs of particle agglomeration. The particle agglomeration may be related to the reduction tem-

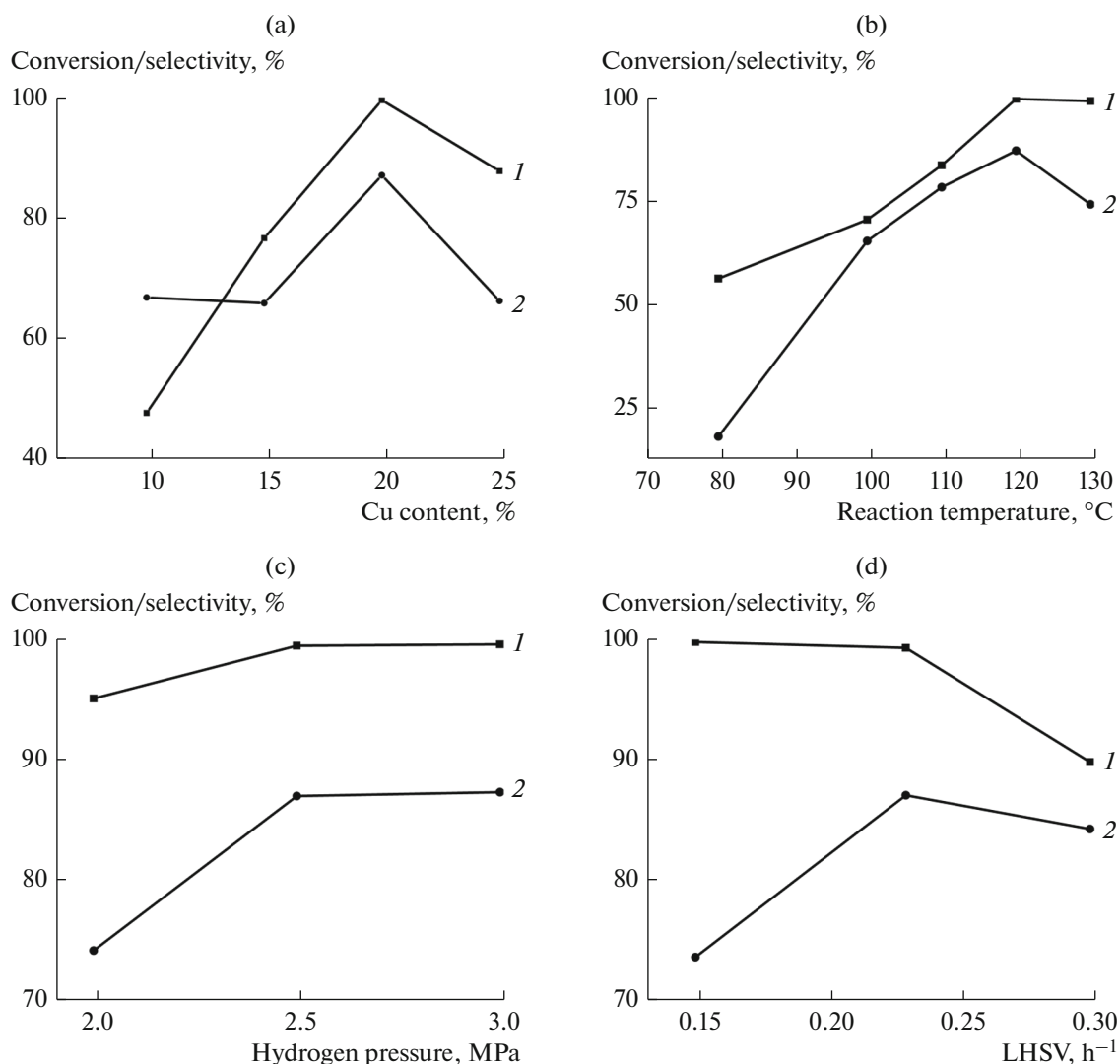


**Fig. 4.** The conversion of NAB (1) and selectivity of BTA (2) as functions of (a) Cu content, (b) reaction temperature, (c) hydrogen pressure, and (d) LHSV. Reaction conditions: (a) temperature 120°C, hydrogen pressure 2.5 MPa, and LHSV 0.23 h<sup>-1</sup>; (b) catalyst 20% Cu/ $\gamma$ -Al<sub>2</sub>O<sub>3</sub>, hydrogen pressure 2.5 MPa, and LHSV 0.23 h<sup>-1</sup>; (c) catalyst 20% Cu/ $\gamma$ -Al<sub>2</sub>O<sub>3</sub>, temperature 120°C, and LHSV 0.23 h<sup>-1</sup>; (d) catalyst 20% Cu/ $\gamma$ -Al<sub>2</sub>O<sub>3</sub>, temperature 120°C, and hydrogen pressure 2.5 MPa. Other conditions: solvent—toluene, base—triethylamine (molar ratio of NAB : triethylamine = 1 : 2).

perature and can affect catalytic performance. The amount of acid sites in the 20% Cu/ $\gamma$ -Al<sub>2</sub>O<sub>3</sub> sample is lower than in other two catalysts, a reduction of acid sites in the catalyst favored the selectivity to BTA. To achieve the optimal reaction performance the activity and selectivity were investigated as functions of the Cu content, reaction temperature, hydrogen pressure and LHSV. The following optimal parameters were chosen: catalyst—20% Cu/ $\gamma$ -Al<sub>2</sub>O<sub>3</sub>, solvent—toluene, base—triethylamine (molar ratio of NAB : triethylamine = 1 : 2). The reactor operates at a temperature of 120°C, a hydrogen pressure of 2.5 MPa, and a LHSV of 0.23 h<sup>-1</sup>. Under the above conditions, the continuous catalytic hydrogenation of NAB pro-

ceeded effectively to yield 87.04% of BTA at 99.52% NAB conversion.

#### ABBREVIATIONS AND NOTATION

|      |   |
|------|---|
| AC   | amino compounds                                 |
| AR   | analytical reagent                              |
| BET  | Brunauer–Emmer–Teller surface area measurements |
| BTA  | 2-(2'-hydroxy-5'-methylphenyl)benzotriazole     |
| HPLC | high performance liquid chromatography          |
| LHSV | liquid hourly space velocity                    |

|                      |   |
|----------------------|---|
| NAB                  | 2-nitro-2'-hydroxy-5'-methylazobenzene              |
| NH <sub>3</sub> -TPD | temperature programmed desorption of ammonia        |
| NO                   | 2-(2'-hydroxy-5'-methylphenyl)benzotriazole N-oxide |
| TEM                  | transmission electron microscopy                    |
| XRD                  | X-ray diffraction                                   |

## FUNDING

This work was supported by the National Natural Science Foundation of China (grant no. 21808161).

## REFERENCES

- Catalán, J., de Paz, J.L.G., Torres, R.M., and Tornero, J.D., *J. Chem. Soc., Faraday Trans.*, 1997, vol. 93, p. 1691.
- Crawford, J.C., *Prog. Polym. Sci.*, 1999, vol. 24, p. 7.
- Jpn. Patent 10045728, 1998.
- WO Patent 2007036948, 2007.
- Jpn. Patent 2004099448, 2004.
- Gostikin, V.P., Lefedova, O.V., Marochko, A.V., and Nemtseva, M.P., *Kinet. Catal.*, 1998, vol. 39, p. 690.
- Koutsimpelis, A.G., Screttas, C.G., and Igglessi-Markopoulou, O., *Heterocycles*, 2005, vol. 65, p. 1393.
- Jin, J., Wen, Z., Long, J., Wang, Y. M., Matsuura, T., and Meng, J.B., *Synth. Commun.*, 2000, vol. 30, p. 829.
- Farkas, R., Torinasi, M., Kolonits, P., Fekete, J., Alonso, O.J., and Novak, L., *Cent. Eur. J. Chem.*, 2010, vol. 8, p. 300.
- Whitmore, W.F., and Revukas, A.J., *J. Am. Chem. Soc.*, 1940, vol. 62, p. 1687.
- Rosevear, J., and Wilshire, J.F.K., *Aust. J. Chem.*, 1982, vol. 35, p. 2089.
- Lefedova, O.V., and Nemtseva, M.P., *Russ. J. Appl. Chem.*, 2012, vol. 85, p. 1128.
- Zuenko, M.A., Nemtseva, M.P., Lefedova, O.V., and Gladkova, E.V., *Russ. J. Phys. Chem.*, 2006, vol. 80, p. 164.
- Lefedova, O.V., Nikolaev, V.N., and Nemtseva, M.P., *Russ. J. Phys. Chem.*, 2003, vol. 77, p. 1059.
- US Patent 3230194, 1966.
- Fr. Patent 2292708, 1976.
- Baik, W., Park, T.H., Kim, B.H., and Jun, Y.M., *J. Org. Chem.*, 1995, vol. 60, p. 5683.
- FRG Patent 3731860, 1988.
- US Patent 3018269, 1962.
- CA Patent 1154779, 1983.
- EP Patent 380839, 1990.
- FRG Patent 2620970, 1976.
- FRG Patent 2455155, 1975.
- Lefedova, O.V., Gostikin, V.P., and Ulitin, M.V., *Russ. J. Phys. Chem.*, 2001, vol. 75, p. 1433.
- Lefedova, O.V., Gostikin, V.P., and Nemtseva, M.P., *Russ. J. Phys. Chem.*, 2001, vol. 75, p. 62.
- Nemtseva, M.P. and Lefedova, O.V., *Kinet. Catal.*, 1994, vol. 35, p. 547.
- Wang, B.W., Fang, W.W., Si, L.L., Li, Y., Yan, X.L., Chen, L.G., and Wang, S.T., *ACS Sustainable Chem. Eng.*, 2015, vol. 3, p. 1890.
- Nemtseva, M.P., Lefedova, O.V., Gostikin, V.P., and Zuenko, M.A., *Russ. J. Phys. Chem.*, 2003, vol. 77, p. 917.
- Wang, B.W., Si, L.L., Yuan, Y.Y., Li, Y., Chen, L.G., and Yan, X.L., *RSC Adv.*, 2016, vol. 6, p. 16766.
- Si, L.L., Wang, B.W., Chen, S.P., Hou, J.R., Yan, X.L., Li, Y., and Chen, L.G., *Catal. Commun.*, 2017, vol. 90, p. 35.
- Kong, X.J. and Chen, L.G., *Catal. Commun.*, 2014, vol. 57, p. 45.
- Kong, X.J., Lai, W.C., Tian, J., Li, Y., Yan, X.L., and Chen, L., *ChemCatChem.*, 2013, vol. 5, p. 2009.
- Kong, X.J. and Chen, L.G., *Appl. Catal., A*, 2014, vol. 476, p. 34.
- Mierczynski, P., Ciesielski, R., Zakrzewski, M., Dawid, B., Mosinska, M., Kedziora, A., Maniukiewicz, W., Dubkov, S., Gromov, D., Szykowska, M., Witonska, I., Shtyka, O., and Maniecki, T., *Kinet. Catal.*, 2018, vol. 59, p. 509.
- Srivastava, S., Jadeja, G.C., and Parikh, J., *J. Mol. Catal. A: Chem.*, 2017, vol. 426, p. 244.
- Artyukha, E.A., Nuzhdin, A.L., Bukhtiyarova, G.A., Derevyannikova, E.A., Gerasimov, E.Y., Gladkii, A.Y., and Bukhtiyarov, V.I., *Kinet. Catal.*, 2018, vol. 59, p. 593.
- Guo, H.T., Gao, R.X., Sun, M.M., Guo, H., Wang, B.W., and Chen, L.G., *ChemSusChem*, 2019, vol. 12, p. 487.
- Kumar, P.S., Korving, L., Keesman, K.J., van Loosdrecht, M.C.M., and Witkamp, G.J., *Chem. Eng. J.*, 2019, vol. 358, p. 160.
- Markov, P.V., Mashkovsky, I.S., Bragina, G.O., Warna, J., Gerasimov, E.Y., Bukhtiyarov, V.I., Stakheev, A.Y., and Murzin, D.Y., *Chem. Eng. J.*, 2019, vol. 358, p. 520.
- Wang, B.W., Si, L.L., Geng, J.Y., Su, Y.H., Li, Y., Yan, X.L., and Chen, L.G., *Appl. Catal., B*, 2017, vol. 204, p. 316.